Enhancement of two-magnon scattering induced by a randomly distributed antiferromagnetic exchange field

Hiroto Sakimura,[1,2] Akio Asami,[2] Takashi Harumoto,[1] Yoshio Nakamura,[1] Ji Shi,[1] and Kazuya Ando[2,*]

[1]*School of Materials and Chemical Technology, Tokyo Institute of Technology, Tokyo 152-8552, Japan*

[2]*Department of Applied Physics and Physico-Informatics, Keio University, Yokohama 223-8522, Japan*

(Received 20 July 2018; revised manuscript received 14 September 2018; published 5 October 2018)

We report a quantitative study of two-magnon scattering in $Ni_{81}Fe_{19}$/NiO bilayers with various NiO thicknesses d_{NiO}. We found that the magnetic damping of the $Ni_{81}Fe_{19}$/NiO bilayer strongly depends on d_{NiO}, which evidences that the amplitude of the two-magnon scattering increases with increasing the thickness of the antiferromagnetic layer. The enhancement of the two-magnon scattering in the $Ni_{81}Fe_{19}$/NiO bilayer is attributed to the increase of randomly distributed antiferromagnetic exchange fields. We calculated the spin-mixing conductance by eliminating the effect of the two-magnon scattering, and found that the value is at 8.1 nm^{-2} for the $Ni_{81}Fe_{19}$/NiO interface. Our result gives further insight on the role of the two-magnon scattering in manipulating magnetic damping, which is crucial for generation and transmission of spin currents in ferromagnet/antiferromagnet systems.

DOI: 10.1103/PhysRevB.98.144406

I. INTRODUCTION

Magnons, the quasiparticle of collective excitation of electrons' spin, show a variety of scattering processes in solids [1]. Such scattering processes are governed by numerous factors, such as dipole/exchange interaction and impurities or defects in crystals. Although a number of experimental and theoretical efforts have been made so far [2–11], further fundamental understanding on the magnon scattering and relaxation processes is still necessary for the development of magnon spintronics and magnonics because it is crucial for the generation and transmission of spin currents in magnetic systems.

Recently, antiferromagnetic materials (AFMs) have attracted increasing interest in spintronics because of their robustness against an external magnetic field and potential for terahertz applications [12–14]. It has been reported that some of AF insulators (AFIs) exhibit highly efficient spin transport properties in ferromagnetic material (FM)/AFI/nonmagnetic metal (NM, e.g., Pt) trilayers [15–24]. In a FM/AFI/NM trilayer, the spin-current transmission from FM to NM can be enhanced, rather than attenuated, by AFI when the thickness of the AFI layer is optimized [15–17]. Its mechanism remains unclear. Furthermore, although numerous works in FM/AFI/NM structures have been conducted, quantitative study of extra magnetic damping induced by interlayer exchange coupling at FM/AFI interfaces, has not been reported yet.

In FM/AFM heterostructures, the magnetization damping of the FM layer has been shown to be affected by two-magnon scattering [5,25]. In the two-magnon scattering, a magnon mode scatters into a different mode with changing its wave number k. Defects and surface pits in a crystal induce this scattering because such crystal disorders break the translational space symmetry, which allows the scattering processes where k is not conserved [1,4,7–9]. Since the magnon scattering strongly affects the spin-current generation from FM [3,6], clarifying the role of the two-magnon scattering in AFI-based systems is indispensable for the fundamental understanding of the generation and transmission of spin currents in antiferromagnetic heterostructures.

In this paper, we investigate the two-magnon scattering in a SiO_2-cap (3 nm)/$Ni_{81}Fe_{19}$ (Py, 8 nm)/NiO (d_{NiO}) layered structure with various d_{NiO}. We measured angular-dependent ferromagnetic resonance (AD-FMR) to extract and separate extrinsic and intrinsic magnetic damping contributions of the Py layer. There are a considerable number of experimental reports on the two-magnon scattering in thin-film ferromagnets [11,26–33]. We here show the possibility to tune the amplitude of the two-magnon scattering by tuning the NiO thickness in the Py/NiO bilayer. Our result shows that the amplitude of the two-magnon scattering can be changed by a factor of more than 10 by tuning the thickness of the NiO layer.

II. EXPERIMENTAL METHODS

The SiO_2-cap (3 nm)/Py (8 nm)/NiO (d_{NiO}) layered structures shown in Fig. 1(a) were fabricated on 10 × 10 mm SiO_2 substrates with NiO thicknesses d_{NiO} = 0–12.5 nm. First, the NiO layer was deposited by radio frequency (RF) magnetron sputtering with a base pressure in 10^{-5} Pa range and Ar pressure of 0.3 Pa during the deposition. We used a NiO target and no oxygen gas was introduced in the chamber for the NiO deposition. After preparing all the NiO films with various d_{NiO}, the 8-nm-thick Py layer was sputtered on all the samples in the same batch. Then, the 3-nm-thick SiO_2 capping layer was sputtered to avoid the surface oxidation

*Correspondence and requests for materials should be addressed to ando@appi.keio.ac.jp.

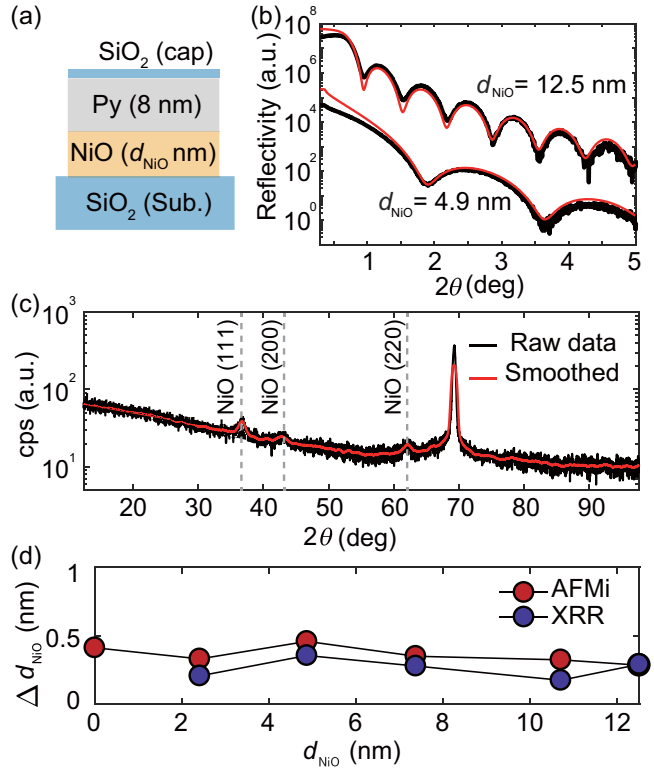

FIG. 1. (a) A schematic illustration of the sample structure. (b) The results of the XRR measurements (black line) and their fitting curves (red line) for the $d_{\mathrm{NiO}} = 4.9$ and 12.5 nm samples. (c) The result of the XRD measurement for the $d_{\mathrm{NiO}} = 72.0$ nm sample. The peak at 2θ around 69° originates from the substrate. The black curve is the raw data and red curve is the smoothed data. (d) NiO thickness d_{NiO} dependence of the NiO surface roughness Δd_{NiO} measured by AFMi (red) and XRR (blue).

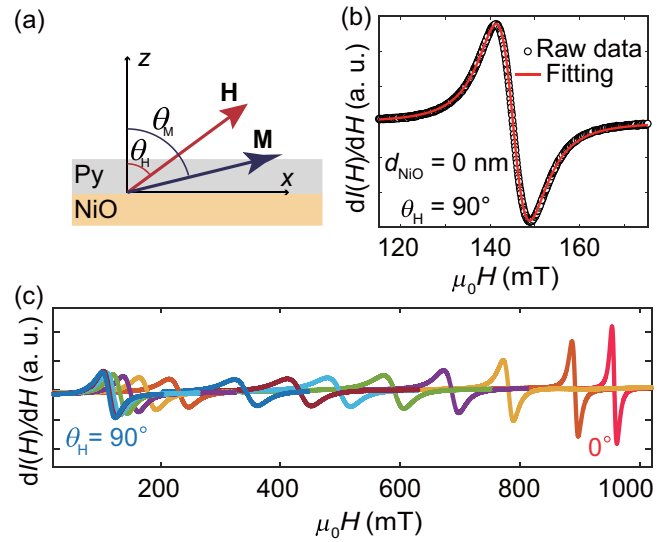

FIG. 2. (a) The measurement geometry of the out-of-plane angular-dependent ferromagnetic resonance (AD-FMR). The definition of the angles, θ_H and θ_M, is also shown. (b) The FMR spectrum for the $d_{\mathrm{NiO}} = 0$ nm sample at $\theta_H = 90°$ (open circles) and its fitting curve (red curve). (c) The FMR spectra for the $d_{\mathrm{NiO}} = 10.7$ nm sample at various θ_H.

of the Py layer in ambient circumstance. All the sputtering processes were performed at room temperature. The thickness and surface roughness of the NiO layer were evaluated by measuring the x-ray reflectometry (XRR) before the Py deposition [Fig. 1(b)]. We also show the x-ray diffractometry (XRD) result in Fig. 1(c). As shown in Fig. 1(c), three peaks from NiO [(111), (220), and (200)] were observed, which unveils the crystallinity of the NiO layer to be polycrystalline. The surface roughness of the NiO layer, or the interface roughness between the NiO and Py layers, was also evaluated using atomic force microscopy (AFMi). The roughness Δd_{NiO} obtained from AFMi is in good agreement with that obtained from XRR, as plotted in Fig. 1(d). This result indicates that the surface roughness of the NiO layer is almost independent of the NiO thickness for $d_{\mathrm{NiO}} < 12.5$ nm.

Figure 2(a) describes the geometry of out-of-plane AD-FMR. The FMR measurements were performed at a fixed microwave frequency of 9.42 GHz and power of 1 mW, while sweeping the external magnetic field H up to 1 T. The magnetic field H was applied at an angle of θ_H from the normal direction of the film plane in this measurement. We conducted the AD-FMR measurement for all the samples within $\theta_H = \pm 90°$. All measurements were performed at room temperature.

III. THEORETICAL BACKGROUND

When the external magnetic field is applied oblique to the film plane, the FMR frequency is expressed as [8–11,34]

$$f_{\mathrm{FMR}} = \frac{\gamma}{2\pi}\sqrt{H_X H_Y}, \tag{1}$$

where

$$H_X = H\cos(\theta_H - \theta_M) - M_{\mathrm{eff}}\cos^2\theta_M, \tag{2}$$

$$H_Y = H\cos(\theta_H - \theta_M) - M_{\mathrm{eff}}\cos(2\theta_M). \tag{3}$$

Here, $\gamma = g\mu_B/\hbar$ is the gyromagnetic ratio and g is the g factor. H is the strength of the external static magnetic field applied at an angle θ_H with respect to the film normal, θ_M is the equilibrium angle of the tipped magnetization M with the film normal as depicted in Fig. 2(a), and $M_{\mathrm{eff}} = H_u + 4\pi M_s$ is the effective magnetization, where $4\pi M_s$ and H_u are the saturation magnetization and the uniaxial out-of-plane anisotropy. In this notation, a positive value of H_u corresponds to the existence of a hard axis to the film normal direction [11].

Equations (1)–(3) assume that no in-plane anisotropy is present in the film. This is reasonable for the macroscopic scale Py/NiO film, since Py is known to exhibit negligible in-plane anisotropy [35], and we did no treatment for exchange bias to appear macroscopically, such as the field cooling and in-field deposition. We also performed VSM magnetometry and confirmed that no sample showed the shift of magnetic hysteresis loop, which indicates the exchange bias is negligibly small in our samples. However, from the microscopic point of view, exchange bias must exist at the Py/NiO interface. Here, the NiO film has antiferromagnetic orientation of magnetization in each grain whose size lies below 20 nm, which does not depend on film thickness as long as

the deposition condition is unchanged [36,37]. They are also randomly distributed over the film due to its polycrystalline nature confirmed by the XRD measurements. Although the sum of all exchange bias from each grain ends up in zero in macroscopic scale, each antiferromagnetic grain in the NiO film can induce in-plane anisotropy on the Py magnetization nearby [38]. The randomly oriented NiO grains form random magnetization alignment in the whole Py film. Thus, this spatially random exchange field acts as a magnetic disorder in the Py film, which can activate two-magnon scattering. We take into account this effect as the fluctuation of H_u to use the well-developed two-magnon scattering analysis [11]. This is reasonable, since H_u is positive for 8-nm Py thin film [39], which means that the magnetization favors an in-plane orientation. How strongly the Py magnetization is stuck in the film plane also depends on the position-dependent microscopic exchange field from each NiO grain, which can be translated to the spatial fluctuation of H_u over the film.

The equilibrium angle of the magnetization θ_M in the Py layer can be calculated by minimizing the free energy F of the system, which takes the simple form, in the absence of the in-plane anisotropy, as

$$F = -M_s H\cos(\theta_H - \theta_M) + \left(\frac{M_s M_{\rm eff}}{2}\right)\sin^2\theta_M. \quad (4)$$

The magnetic damping with different origins show distinct contributions to the θ_H dependence of the peak-to-peak FMR linewidth. We use the formulation presented by Arias and Mills [8–11]. The peak-to-peak FMR linewidth $\mu_0\Delta H$ is expressed as

$$\mu_0\Delta H = \mu_0\Delta H_{\rm G} + \mu_0\Delta H_{\rm inhomo} + \mu_0\Delta H_{\rm TMS}. \quad (5)$$

The first term is the intrinsic linewidth due to the Gilbert damping, which is proportional to the microwave frequency f and written as

$$\mu_0\Delta H_{\rm G} = \frac{2}{\sqrt{3}}\frac{2\pi f}{\gamma\,\Xi}\alpha, \quad (6)$$

where α is the Gilbert damping constant and Ξ is the dragging function given by

$$\Xi = \cos(\theta_H - \theta_M) - \frac{3H_X + H_Y}{H_Y(H_X + H_Y)}H\sin^2(\theta_H - \theta_M). \quad (7)$$

$\mu_0\Delta H_{\rm G}$ is enhanced when the magnetization direction is not parallel to the external magnetic field, $\theta_H \neq \theta_M$ [8–11]. This effect is known as the field dragging effect induced by magnetic anisotropy fields acting on the magnetization vector [4,5,11,25–27]. This dragging function becomes unity when the external field and the magnetization vector are aligned parallel to each other ($\theta_H = \theta_M$), which requires certain magnitude of external field that is large enough to make the equilibrium magnetization parallel to the external field. Once this condition is satisfied, the peak-to-peak linewidth at $\theta_H = 0^\circ$ (field applied to out-of-plane) is expected to be equal to that of at $\theta_H = \pm 90^\circ$ (field applied in the film plane) in the absence of extrinsic contributions to the linewidth.

The second term describes the contribution of the anisotropy dispersion for the out-of-plane direction, written as

$$\Delta H_{\rm inhomo} = \left|\frac{dH_{\rm res}}{dM_{\rm eff}}\right|\Delta M_{\rm eff} + \left|\frac{dH_{\rm res}}{d\theta_H}\right|\Delta\theta_H, \quad (8)$$

where $\Delta M_{\rm eff}$ and $\Delta\theta_H$ represent the dispersion of magnitude and direction of $M_{\rm eff}$. These are caused by the local variation of magnitude and the direction of $M_{\rm eff}$ through the local variation of $H_{\rm res}$ [34,40,41].

The third term in Eq. (5) is the contribution of the two-magnon scattering induced by surface defects and is given as

$$\Delta H_{\rm TMS} = \frac{2}{\sqrt{3}}\Gamma(H,\theta_H)\sin^{-1}\sqrt{\frac{-H_X}{H_X + M_{\rm eff}}\frac{\cos(2\theta_M)}{\sin^2\theta_M}}. \quad (9)$$

The coefficient $2/\sqrt{3}$ was multiplied to adjust the theory to the peak-to-peak linewidth defined in the present study. Here, $\Gamma(H,\theta_H)$ is given by

$$\begin{aligned}\Gamma(H,\theta_H) = \frac{C_{\rm TMS}}{(H_X + H_Y)^2\,\Xi}\Big\{&\left(\left\langle\frac{c}{a}\right\rangle - 1\right)H_Y^2 \\ &+\left(\left\langle\frac{a}{c}\right\rangle - 1\right)[H_Y\sin^2\theta_M - H_X\cos(2\theta_M)]^2 \\ &+[H_X\cos(2\theta_M) + H_Y\cos^2\theta_M]^2\Big\}, \end{aligned} \quad (10)$$

where $C_{\rm TMS} = 8H_u^2 b^2 p/\pi D$ represents the amplitude of the two-magnon scattering, whose unit is the same as H_u. D is the exchange stiffness of the Py layer. The defects are supposed to cover the film with the ratio of p and assumed to be rectangular in nature with the aspect ratio of a/c and height (or depth) b. The brackets $\langle\rangle$ express the average of lateral dimension, since a and c must have random distribution [8,9]. The contribution of the two-magnon scattering disappears when $\theta_M < 45^\circ$; in Eq. (9), the inside of the square root becomes negative in this range. This indicates that when the measured linewidth of the perpendicular geometry ($\theta_H = \theta_M = 0^\circ$) is smaller than that of the in-plane geometry ($\theta_H = \theta_M = 90^\circ$), the result demonstrates that the two-magnon scattering does contribute to overall relaxation process [8,9,11].

The two-magnon scattering is known to be activated by the random fluctuation of uniaxial anisotropy H_u, surface/interface roughness, and defects [8–11,33]. The contribution from the latter factors results in the random fluctuation of the direction of H_u, which can also be taken into account in the analysis performed in Ref. [11]. We assume that the random fluctuation of H_u is enhanced by randomly oriented exchange bias induced by statistical distribution of AF grains in polycrystalline NiO [38] and the validity of this discussion will be confirmed below.

IV. RESULTS AND DISCUSSION

An FMR spectrum for the Py/NiO bilayer with $d_{\rm NiO} = 0$ nm measured at $\theta_H = 90^\circ$ is shown in Fig. 2(b). By fitting the measured curve using the first derivative of a Lorentz function, we determined the resonance field $\mu_0 H_{\rm res}$ and the peak-to-peak linewidth $\mu_0\Delta H$. Figure 2(c) shows the FMR spectra for the Py/NiO bilayer with $d_{\rm NiO} = 10.7$ nm at various θ_H. We can see the variation of peak-to-peak linewidth $\mu_0\Delta H$, as well as the shift of the resonance field $\mu_0 H_{\rm res}$.

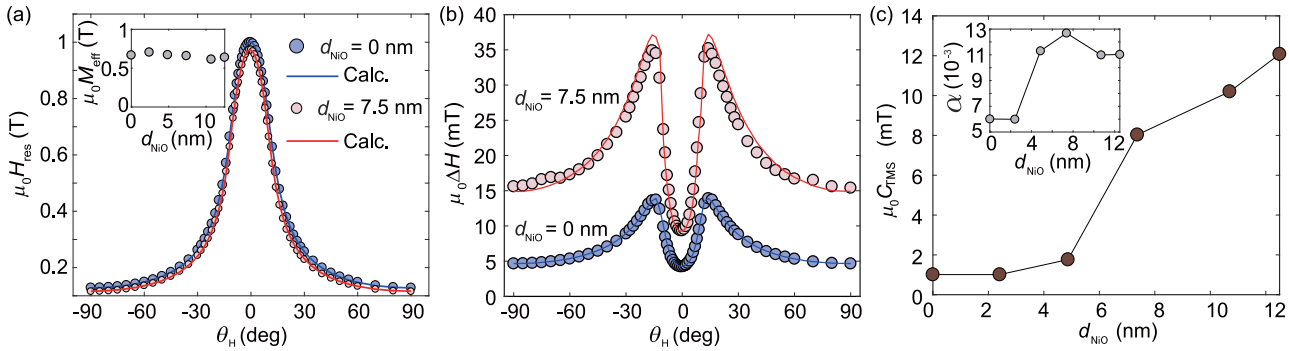

FIG. 3. (a) θ_H dependence of the resonance field $\mu_0 H_{res}$ for the $d_{NiO} = 0$ and 7.5 nm samples. The red and blue curves are the results of the numerical calculation. The inset is the d_{NiO} dependence of effective magnetization M_{eff}. (b) θ_H dependence of the total the peak-to-peak linewidth $\mu_0 \Delta H$ for the $d_{NiO} = 0$ and 7.5 nm samples (blue and red solid circles) and their fitting curves (blue and red curves). (c) d_{NiO} dependence of the amplitude of the two-magnon scattering C_{TMS} extracted from the fitting shown in (b). Here, μ_0 was multiplied to adjust the unit. The inset shows d_{NiO} dependence of the Gilbert damping constant α.

Figure 3(a) shows the θ_H dependence of the resonance field $\mu_0 H_{res}$ for the Py/NiO bilayer with $d_{NiO} = 0$ and 7.5 nm. The FMR field is maximized when the external field is applied perpendicular to the film plane, $\theta_H = 0^\circ$. $\mu_0 H_{res}$ vs θ_H was calculated numerically using Eqs. (1)–(4) and was fitted to the experimental results by adjusting the values of effective magnetization M_{eff} and g factor g. Using the values of M_{eff} and g obtained from the $\mu_0 H_{res}$ vs θ_H, $\mu_0 \Delta H$ vs θ_H was then calculated using Eqs. (1)–(10) with fitting parameters α, ΔM_{eff}, $\Delta\theta_H$, and C_{TMS}. For the calculation, a/c has been fixed at $1.7/1.1 \simeq 1.545$ for all the Py/NiO films with various d_{NiO} to provide the best fitting results, which confirms that the grain dimension does not depend on d_{NiO}. These experimental results and numerical fitting results are shown in Fig. 3(b) for $d_{NiO} = 0$ and 7.5 nm.

The most notable feature of Fig. 3(b) is that the linewidth $\mu_0 \Delta H$ of the perpendicular geometry $\theta_H = 0$ is obviously smaller than that of the in-plane geometry $\theta_H = 90^\circ$ in the Py/NiO film with $d_{NiO} = 7.5$ nm. This result demonstrates that the two-magnon scattering becomes significant by attaching the NiO layer to the Py film. In fact, the amplitude of the two-magnon scattering, C_{TMS}, increases with d_{NiO}, as shown in Fig. 3(c). There are two possible origins of this behavior. The first candidate is the increase of the interface roughness and surface pits of the Py layer. However, this possibility can be excluded; as shown in Fig. 1(d), the NiO surface, or the Py/NiO interface, roughness is independent of d_{NiO}. We also note that the difference in the level of defects and surface pits in the Py layers should be negligible because the Py layer was fabricated in the same batch. This is evidenced by the d_{NiO}-independent M_{eff} shown in the inset of Fig. 3(a).

The remaining possibility that can explain the enhanced two-magnon scattering with d_{NiO} is the increased fluctuation of H_u due to the interfacial exchange field produced by the NiO, since the exchange bias in FM/AFM bilayers is known to be affected by the thickness and grain size of the antiferromagnetic layer [37,42]. From the result shown in Fig. 1(d) and the parameters extracted from the AD-FMR, it is reasonable to assume that the grain sizes of the NiO layer in the Py/NiO bilayer are almost unchanged by changing d_{NiO} [36,37]. Therefore, the only factor that amplifies the interfacial exchange field is NiO thickness [38]. Although the AFM thickness dependence of the exchange field is nontrivial, it is widely accepted that the exchange field becomes larger with increasing the NiO thickness when $d_{AFM} < 45$ nm [43]. This results in the larger fluctuation of H_u over the sample and hence enhances the contribution of the two-magnon scattering to the total $\mu_0 \Delta H$. Here, we mean the microscopic size as the order of grain sizes in the NiO layer. Because of the polycrystalline nature of NiO, confirmed by XRD [Fig. 1(c)], the direction of the interfacial exchange field is supposed to have random orientation grain by grain, since the grains are not magnetically coupled to each other in NiO and hence behave independently [38]. In addition, VSM measurements revealed no sample used in this study has macroscopic exchange bias. Although the macroscopic exchange bias is negligible due to the random distribution of the antiferromagnetic grain, the exchange field does exist for each grain as long as the temperature is lower than the blocking temperature of NiO [38]. Figure 3(c) shows that the two-magnon scattering is negligible despite the presence of the NiO layer for $d_{NiO} = 2.4$ nm. This is consistent with the above scenario, since the blocking temperature (as well as the Néel temperature) of NiO with $d_{NiO} = 2.4$ nm is lower than room temperature [15,24,44,45], thus no interfacial exchange field is expected. Gradual growth of C_{TMS} at $d_{NiO} = 4.9$ nm indicates the appearance of the exchange field from the NiO layer, which is consistent with the fact that the blocking temperature of a NiO film with $d_{NiO} \sim 5$ nm is above room temperature [46]. Nonzero value of C_{TMS} at $d_{NiO} = 0$ nm can be attributed to the existence of finite crystal disorders, such as defects in the Py layer, and this effect is present in all the thickness range. The inset of Fig. 3(c) shows d_{NiO} dependence of the intrinsic Gilbert damping constant α. α increases with d_{NiO}, which reflects the effect of spin pumping induced by the attachment of NiO [47] and allows us to evaluate the spin-mixing conductance $g^{\uparrow\downarrow}$.

The spin-mixing conductance $g^{\uparrow\downarrow}$ refers to the efficiency with which the spin currents across the Py/NiO interface are generated [48]. In the presence of the spin pumping and two-magnon scattering, the FMR linewidth of the Py/NiO bilayer

$\mu_0\Delta H_{\mathrm{Py/NiO}}$ at $\theta_H = 90^\circ$ can be expressed as

$$\begin{aligned}\mu_0\Delta H_{\mathrm{Py/NiO}} &= \mu_0\Delta H_{\mathrm{Py}} + \mu_0\Delta H_{\mathrm{add}} \\ &= \mu_0\Delta H_{\mathrm{Py}} + \mu_0\Delta H_{\mathrm{SP}} + \mu_0\Delta H_{\mathrm{TMS}}, \end{aligned} \quad (11)$$

where $\mu_0\Delta H_{\mathrm{Py}}$ is the FMR linewidth of a Py film, which includes $\mu_0\Delta H_{\mathrm{inhomo}}$ in Eq. (5) and can be obtained from the experimental data of $d_{\mathrm{NiO}} = 0\,\mathrm{nm}$, and $\mu_0\Delta H_{\mathrm{add}}$ is the additional linewidth induced by attaching the NiO layer. Here, $\mu_0\Delta H_{\mathrm{add}}$ is comprised of $\mu_0\Delta H_{\mathrm{TMS}}$ and $\mu_0\Delta H_{\mathrm{SP}}$, the additional linewidth due to the two-magnon scattering and spin pumping, respectively. The latter, $\mu_0\Delta H_{\mathrm{SP}}$, is proportional to the additional damping due to the spin pumping [49,50],

$$\Delta\alpha_{\mathrm{SP}} = \frac{g\mu_{\mathrm{B}}}{4\pi M_{\mathrm{S}} d_{\mathrm{F}}} g_{\mathrm{eff}}^{\uparrow\downarrow}, \quad (12)$$

as $\mu_0\Delta H_{\mathrm{SP}} = (2/\sqrt{3})(2\pi f)/\gamma\,\Delta\alpha_{\mathrm{SP}}$, where $g_{\mathrm{eff}}^{\uparrow\downarrow}$ is the effective spin-mixing conductance. In previous studies, the effective spin-mixing conductance $g_{\mathrm{eff}}^{\uparrow\downarrow}$ of ferromagnetic metal/heavy-metal bilayers, such as a Py/Pt bilayer, has often been directly estimated from the additional linewidth $\mu_0\Delta H_{\mathrm{add}}$ induced by attaching the heavy-metal layer. However, this procedure is reasonable only when $\mu_0\Delta H_{\mathrm{add}} = \mu_0\Delta H_{\mathrm{SP}}$. For the Py/NiO bilayer, $\mu_0\Delta H_{\mathrm{add}} = \mu_0\Delta H_{\mathrm{SP}} + \mu_0\Delta H_{\mathrm{TMS}} \neq \mu_0\Delta H_{\mathrm{SP}}$ because of the fact that the additional linewidth due to the two-magnon scattering, $\mu_0\Delta H_{\mathrm{TMS}}$, cannot be neglected. Thus, to determine the effective spin-mixing conductance $g_{\mathrm{eff}}^{\uparrow\downarrow}$ of the Py/NiO bilayer, it is necessary to calculate $\mu_0\Delta H_{\mathrm{SP}}$ by subtracting $\mu_0\Delta H_{\mathrm{TMS}}$ from the measured values of $\mu_0\Delta H_{\mathrm{add}}$.

In Fig. 4(a), we show d_{NiO} dependence of the FMR linewidth $\mu_0\Delta H_{\mathrm{Py/NiO}}$ at $\theta_{\mathrm{H}} = 90^\circ$ for the Py/NiO bilayer (red circles). To clarify the importance of taking into account the two-magnon scattering for the estimation of the effective spin-mixing conductance $g_{\mathrm{eff}}^{\uparrow\downarrow}$, we first calculated $g_{\mathrm{eff}}^{\uparrow\downarrow}$ by neglecting the additional linewidth $\mu_0\Delta H_{\mathrm{TMS}}$ due to the two-magnon scattering. The red circles in Fig. 4(b) show $g_{\mathrm{eff}}^{\uparrow\downarrow}$ calculated by neglecting $\mu_0\Delta H_{\mathrm{TMS}}$, or assuming $\mu_0\Delta H_{\mathrm{add}} = \mu_0\Delta H_{\mathrm{SP}}$, as a function of ϕ defined as

$$g_{\mathrm{eff}}^{\uparrow\downarrow} = g^{\uparrow\downarrow}\frac{1}{1 + [2\sqrt{\epsilon/3}\tanh(d_{\mathrm{NiO}}/\lambda)]^{-1}} = g^{\uparrow\downarrow}\phi, \quad (13)$$

where $g^{\uparrow\downarrow}$ is the mixing conductance. For the calculation, we used

$$g_{\mathrm{eff}}^{\uparrow\downarrow} = \frac{4\pi M_{\mathrm{S}}}{g\mu_{\mathrm{B}}}\frac{\sqrt{3}}{2}\frac{\gamma}{2\pi f}\mu_0\Delta H_{\mathrm{add}}, \quad (14)$$

for $d_{\mathrm{NiO}} \geqslant 4.9\,\mathrm{nm}$ and assumed the spin diffusion length of NiO $\lambda = 9.8\,\mathrm{nm}$ [15,17], $\epsilon = 0.01$ and $4\pi M_{\mathrm{S}} \simeq M_{\mathrm{eff}}$ [47,51]. We did not use the data at $d_{\mathrm{NiO}} = 2.4\,\mathrm{nm}$, since the NiO layer is not antiferromagnetic but paramagnetic at room temperature at this thickness due to finite-size effect [21,24]. The red circles in Fig. 4(b) show that the estimated $g_{\mathrm{eff}}^{\uparrow\downarrow}$ is not proportional to ϕ, which is inconsistent with the model of the spin pumping: $g_{\mathrm{eff}}^{\uparrow\downarrow} = g^{\uparrow\downarrow}\phi$ [49,50]. The reason for this inconsistency is that the thickness-dependent $\mu_0\Delta H_{\mathrm{TMS}}$ is neglected in this calculation, leading to overestimation of $g_{\mathrm{eff}}^{\uparrow\downarrow}$.

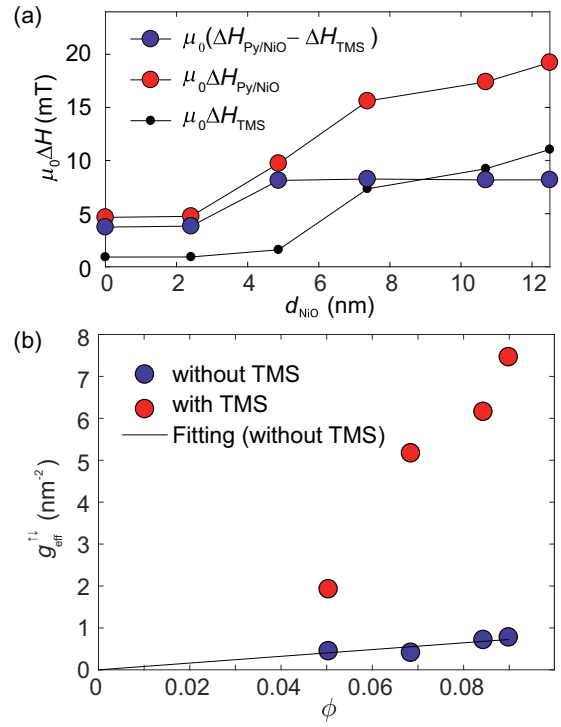

FIG. 4. (a) Experimentally obtained spectral linewidth at $\theta_H = 90^\circ$ (red), TMS-originated linewidth calculated from Eq. (9) (black) and the difference of these two (blue). (b) Effective spin-mixing conductance $g_{\mathrm{eff}}^{\uparrow\downarrow}$ plotted with ϕ defined in Eq. (13). The slope for blue plots correspond to the spin-mixing conductance $g^{\uparrow\downarrow}$.

To determine the spin-mixing conductance of the Py/NiO bilayer, we calculated the additional linewidth $\mu_0\Delta H_{\mathrm{SP}}$ at $\theta_{\mathrm{H}} = 90^\circ$ due to the spin pumping (the blue circles in Fig. 4(a), which include $\mu_0\Delta H_{\mathrm{Py}}$) using $\mu_0\Delta H_{\mathrm{SP}} = \mu_0\Delta H_{\mathrm{add}} - \mu_0\Delta H_{\mathrm{TMS}}$ as shown in Fig. 4(a). Here, the additional linewidth due to the two-magnon scattering $\mu_0\Delta H_{\mathrm{TMS}}$ at $\theta_{\mathrm{H}} = 90^\circ$ was calculated using the parameter shown in Fig. 3(c). Using the calculated $\mu_0\Delta H_{\mathrm{SP}}$, we obtained $g_{\mathrm{eff}}^{\uparrow\downarrow}$ using Eq. (14) as shown in Fig. 4(b) (the blue circles). This result shows that $g_{\mathrm{eff}}^{\uparrow\downarrow}$ is proportional to ϕ, consistent with the model of the spin pumping. From the linear fitting to this result, we obtained $g_{\mathrm{eff}}^{\uparrow\downarrow} = 8.1\,\mathrm{nm}^{-2}$. This is a reasonable value, consistent with the result of Ikebuchi *et al.* [47]. This result indicates that it is indispensable to take into account the two-magnon scattering effect to determine the spin-mixing conductance at ferromagnet/antiferromagnet interfaces.

V. CONCLUSIONS

We performed AD-FMR measurements for Py/NiO bilayers with various NiO thickness, d_{NiO}. The magnetic damping parameter was determined from the θ_H dependence of the peak-to-peak FMR linewidth for each film. We found that the FMR linewidth due to the two-magnon scattering became significant with increasing d_{NiO}. This result indicates that the random interfacial exchange magnetic field produced by the NiO layer is the origin of the enhanced two-magnon scattering; the local exchange coupling induces the increase

of the fluctuation of the anisotropy field H_u in the Py layer, resulting in the enhancement of the magnetic disorder, which can be taken into account as nonperiodic perturbation. The spin-mixing conductance $g^{\uparrow\downarrow}$ was calculated based on the spin pumping theory by eliminating the contribution from two-magnon scattering. The calculated $g^{\uparrow\downarrow} = 8.1\,\mathrm{nm}^{-2}$ is in good agreement with previously reported value, which indicates the significant role of the two-magnon scattering effect for the determination of spin-mixing conductance at ferromagnet/antiferromagnet interfaces. The results presented in this study offer a way to tune the two-magnon scattering amplitude in FM by controlling the thickness of an adjacent antiferromagnetic layer.

ACKNOWLEDGMENTS

This work was supported by JSPS KAKENHI Grants No. 26220604, No. 26103004, the Asahi Glass Foundation, JSPS Core-to-Core Program, and Spintronics Research Network of Japan (Spin-RNJ). H.S. is supported by JSPS Grant-in-Aid for Research Fellowship for Young Scientists (DC1) No. 17J03624.

[1] H. Suhl and G. T. Rado (eds.), *Magnetism* (Academic Press, New York, 1963).
[2] S. Jiang, L. Sun, Y. Yin, Y. Fu, C. Luo, Y. Zhai, and H. Zhai, AIP Advances **7**, 056029 (2017).
[3] H. Sakimura, T. Tashiro, and K. Ando, Nature Commun. **5**, 5730 (2014).
[4] H. Kurebayashi, T. Skinner, K. Khazen, K. Olejník, D. Fang, C. Ciccarelli, R. Campion, B. Gallagher, L. Fleet, A. Hirohata *et al.*, Appl. Phys. Lett. **102**, 062415 (2013).
[5] B. K. Kuanr, R. Camley, and Z. Celinski, J. Appl. Phys. **93**, 7723 (2003).
[6] H. Kurebayashi, O. Dzyapko, V. E. Demidov, D. Fang, A. J. Ferguson, and S. O. Demokritov, Nature Mater. **10**, 660 (2011).
[7] M. Hurben and C. Patton, J. Appl. Phys. **83**, 4344 (1998).
[8] R. Arias and D. L. Mills, Phys. Rev. B **60**, 7395 (1999).
[9] R. Arias and D. Mills, J. Appl. Phys. **87**, 5455 (2000).
[10] P. Landeros, R. E. Arias, and D. L. Mills, Phys. Rev. B **77**, 214405 (2008).
[11] J. Lindner, I. Barsukov, C. Raeder, C. Hassel, O. Posth, R. Meckenstock, P. Landeros, and D. L. Mills, Phys. Rev. B **80**, 224421 (2009).
[12] R. Khymyn, I. Lisenkov, V. Tiberkevich, B. A. Ivanov, and A. Slavin, Sci. Rep. **7**, 43705 (2017).
[13] H. V. Gomonay and V. M. Loktev, Phys. Rev. B **81**, 144427 (2010).
[14] P. Wadley, B. Howells, J. Železný, C. Andrews, V. Hills, R. P. Campion, V. Novák, K. Olejník, F. Maccherozzi, S. Dhesi *et al.*, Science **351**, 587 (2016).
[15] H. Wang, C. Du, P. C. Hammel, and F. Yang, Phys. Rev. Lett. **113**, 097202 (2014).
[16] C. Hahn, G. De Loubens, V. V. Naletov, J. B. Youssef, O. Klein, and M. Viret, Europhys. Lett. **108**, 57005 (2014).
[17] H. Wang, C. Du, P. C. Hammel, and F. Yang, Phys. Rev. B **91**, 220410 (2015).
[18] T. Shang, Q. Zhan, H. Yang, Z. Zuo, Y. Xie, L. Liu, S. Zhang, Y. Zhang, H. Li, B. Wang *et al.*, Appl. Phys. Lett. **109**, 032410 (2016).
[19] T. Moriyama, S. Takei, M. Nagata, Y. Yoshimura, N. Matsuzaki, T. Terashima, Y. Tserkovnyak, and T. Ono, Appl. Phys. Lett. **106**, 162406 (2015).
[20] D. Hou, Z. Qiu, J. Barker, K. Sato, K. Yamamoto, S. Vélez, J. M. Gomez-Perez, L. E. Hueso, F. Casanova, and E. Saitoh, Phys. Rev. Lett. **118**, 147202 (2017).
[21] Z. Qiu, J. Li, D. Hou, E. Arenholz, A. Tan, K.-i. Uchida, K. Sato, S. Okamoto, Y. Tserkovnyak, Z. Qiu *et al.*, Nature Commun. **7**, 12670 (2016).
[22] Z. Qiu, D. Hou, J. Barker, K. Yamamoto, O. Gomonay, and E. Saitoh, Nature Mater. **17**, 577 (2018).
[23] L. Frangou, S. Oyarzún, S. Auffret, L. Vila, S. Gambarelli, and V. Baltz, Phys. Rev. Lett. **116**, 077203 (2016).
[24] W. Lin and C. L. Chien, Phys. Rev. Lett. **118**, 067202 (2017).
[25] K. Sun, Y. Yang, Y. Liu, Z. Yu, Y. Zeng, W. Tong, X. Jiang, Z. Lan, R. Guo, and C. Wu, IEEE Trans. Magn. **51**, 2006304 (2015).
[26] I. Barsukov, P. Landeros, R. Meckenstock, J. Lindner, D. Spoddig, Z.-A. Li, B. Krumme, H. Wende, D. L. Mills, and M. Farle, Phys. Rev. B **85**, 014420 (2012).
[27] J. Dubowik, K. Zaleski, H. Glowinski, and I. Goscianska, Phys. Rev. B **84**, 184438 (2011).
[28] K. Zakeri, J. Lindner, I. Barsukov, R. Meckenstock, M. Farle, U. Von Hörsten, H. Wende, W. Keune, J. Rocker, S. Kalarickal *et al.*, Phys. Rev. B **76**, 104416 (2007).
[29] K. Lenz, H. Wende, W. Kuch, K. Baberschke, K. Nagy, and A. Jánossy, Phys. Rev. B **73**, 144424 (2006).
[30] G. Woltersdorf, M. Buess, B. Heinrich, and C. H. Back, Phys. Rev. Lett. **95**, 037401 (2005).
[31] R. D. McMichael, M. D. Stiles, P. J. Chen, and W. F. Egelhoff Jr, Phys. Rev. B **58**, 8605 (1998).
[32] R. D. McMichael, M. D. Stiles, P. Chen, and W. F. Egelhoff Jr., J. Appl. Phys. **83**, 7037 (1998).
[33] A. Azevedo, A. B. Oliveira, F. M. de Aguiar, and S. M. Rezende, Phys. Rev. B **62**, 5331 (2000).
[34] S. Mizukami, Y. Ando, and T. Miyazaki, Phys. Rev. B **66**, 104413 (2002).
[35] H. Gong, M. Rao, D. E. Laughlin, and D. N. Lambeth, J. Appl. Phys. **85**, 5750 (1999).
[36] H.-L. Chen, Y.-M. Lu, and W.-S. Hwang, Thin Solid Films **498**, 266 (2006).
[37] G. Vallejo-Fernandez, L. Fernandez-Outon, and K. O'Grady, J. Phys. D **41**, 112001 (2008).
[38] K. O'Grady, L. Fernandez-Outon, and G. Vallejo-Fernandez, J. Magn. Magn. Mater. **322**, 883 (2010).
[39] J. O. Rantschler, P. Chen, A. S. Arrott, R. D. McMichael, W. F. Egelhoff Jr, and B. B. Maranville, J. Appl. Phys. **97**, 10J113 (2005).
[40] S. Mizukami, Y. Ando, and T. Miyazaki, J. J. Appl. Phys. **40**, 580 (2001).
[41] S. Mizukami, Y. Ando, and T. Miyazaki, J. Magn. Magn. Mater. **226**, 1640 (2001).
[42] K. Takano, R. Kodama, A. Berkowitz, W. Cao, and G. Thomas, J. Appl. Phys. **83**, 6888 (1998).
[43] J. R. Fermin, Revista Mexicana de Física **63**, 145 (2017).

[44] M. Gruyters, J. Magn. Magn. Mater. **248**, 248 (2002).
[45] A. Baruth and S. Adenwalla, Phys. Rev. B **78**, 174407 (2008).
[46] X. Lang, W. Zheng, and Q. Jiang, Nanotechnology **18**, 155701 (2007).
[47] T. Ikebuchi, T. Moriyama, H. Mizuno, K. Oda, and T. Ono, Appl. Phys. Exp. **11**, 073003 (2018).
[48] Z. Qiu, K. Ando, K. Uchida, Y. Kajiwara, R. Takahashi, H. Nakayama, T. An, Y. Fujikawa, and E. Saitoh, Appl. Phys. Lett. **103**, 092404 (2013).
[49] O. Mosendz, J. E. Pearson, F. Y. Fradin, G. E. W. Bauer, S. D. Bader, and A. Hoffmann, Phys. Rev. Lett. **104**, 046601 (2010).
[50] Y. Tserkovnyak, A. Brataas, G. E. Bauer, and B. I. Halperin, Rev. Mod. Phys. **77**, 1375 (2005).
[51] K. Ando, S. Takahashi, J. Ieda, Y. Kajiwara, H. Nakayama, T. Yoshino, K. Harii, Y. Fujikawa, M. Matsuo, S. Maekawa *et al.*, J. Appl. Phys. **109**, 103913 (2011).